

Simulating Neutron Star Mergers as r-process Sources in Ultra Faint Dwarf Galaxies

Mohammadtaher Safarzadeh[★] & Evan Scannapieco

School of Earth and Space Exploration, Arizona State University, Tempe, AZ 85287-1404, USA

22 March 2022

ABSTRACT

To explain the high observed abundances of r-process elements in local ultra-faint dwarf (UFD) galaxies, we perform cosmological zoom simulations that include r-process production from neutron star mergers (NSMs). We model star-formation stochastically and simulate two different halos with total masses $\approx 10^8 M_{\odot}$ at $z = 6$. We find that the final distribution of [Eu/H] vs. [Fe/H] is relatively insensitive to the energy by which the r-process material is ejected into the interstellar medium, but strongly sensitive to the environment in which the NSM event occurs. In one halo the NSM event takes place at the center of the stellar distribution, leading to high-levels of r-process enrichment such as seen in a local UFD, Reticulum II (Ret II). In a second halo, the NSM event takes place outside of the densest part of the galaxy, leading to a more extended r-process distribution. The subsequent star formation occurs in an interstellar medium with shallow levels of r-process enrichment which results in stars with low levels of [Eu/H] compared to Ret II stars even when the maximum possible r-process mass is assumed to be ejected. This suggests that the natal kicks of neutron stars may also play an important role in determining the r-process abundances in UFD galaxies, a topic that warrants further theoretical investigation.

Key words: Stars: Neutron – Galaxies: Dwarf – Stars: abundances

1 INTRODUCTION

The production of elements heavier than zinc requires events with high fluxes of neutrons. These particles are captured by lighter nuclei at a rate that is slow or rapid with respect to subsequent beta decays, leading to neutron-capture processes labeled s or r, respectively (Burbidge et al. 1957; Sneden & Cowan 2003; Sneden et al. 2008). While the production of s-process elements for heavy elements with $A > 90$ is thought to primarily occur in asymptotic giant branch stars (Busso et al. 1999), r-process elements could be formed in core-collapse supernovae (SNcc) or in neutron star mergers (NSMs), with an ongoing debate regarding the dominance of one mechanism over the other (Argast et al. 2004). A key difference between these mechanisms is the number of events required to produce the abundances observed today. Coalescing NSMs are calculated to eject $10^{-3} - 10^{-2} M_{\odot}$ of r-process matter (Rosswog et al. 1999, 2000), which is orders of magnitude larger than the $10^{-6} - 10^{-5} M_{\odot}$ ejected by SNcc, but their rate is also significantly lower than core-collapse

rates (Cowan et al. 1991; Woosley et al. 1994; Kuroda et al. 2008; Wanajo 2013).

One discriminant between these two models is the abundance of r-process elements found within local ultra-faint dwarf galaxies (UFDs, Brown et al. 2012; Frebel & Bromm 2012; Vargas et al. 2013) discovered in deep wide-area sky surveys (Koposov et al. 2015a,b; Bechtol et al. 2015). Recently Ji et al. (2016) obtained high-resolution spectra of nine stars in the local UFD Reticulum II (Ret II), and found that SNcc are unable to account for the observed high r-process element abundances in this galaxy. Instead, a rare event such as a NSM (Tanvir et al. 2013; Wallner et al. 2015) or a magnetorotationally-driven supernova (SN) (Winteler et al. 2012; Wehmeyer et al. 2015; Nishimura et al. 2015) is required to explain the observed high stellar abundances of Eu and Ba.

Other constraints on the production of r-process elements have been obtained through studies of the Milky Way (MW) halo. van de Voort et al. (2015) carried out a zoom simulation of a MW like halo at $z = 0$ and concluded that NSM events can explain the observed [r-process/Fe] abundance ratios assuming $10^{-2} M_{\odot}$ r-process mass is ejected into

[★] E-mail: mts@asu.edu

the ISM in each NSM event. [Shen et al. \(2015\)](#) studied the sites of r-process production by post-processing “Eris” zoom simulations at $z = 0$. They found that r-process elements can be incorporated into low metallicity stars at very early times, a result that is rather insensitive to modest variations in delay times, the delay distribution, and merger rates.

In this study, we focus on simulating one NSM event in the star formation history of two UFD candidates at high redshifts and compare these results with local observations. We simulate two different halos: one in which star formation begins at $z \approx 13$ and another in which star formation begins at $z \approx 8$, which is consistent with the suggested wide redshift range for reionization to quench the star formation in UFDs ([Brown et al. 2014](#)). We study the statistics of the NSM event in terms of three key parameters: the coalescence time of the two merging neutron stars, the energy associated with the event, and the mass of r-process material that is released into the ISM. These results provide joint constraints that can be used to rule out or provide support for currently favored models for the sources producing r-process elements.

The paper is organized as follows: In §2 we present the setup of the zoom simulations. In §3 we present our results on the r-process abundance of the gas and stellar content of the galaxies and in §4 we discuss the implications and give conclusions.

2 SIMULATION SETUP

We use RAMSES ([Teyssier 2002](#)), a cosmological adaptive mesh refinement (AMR) code, which implements an unsplit second-order Godunov scheme for evolving the Euler equations. RAMSES variables are cell-centered and interpolated to the cell faces for flux calculations, which are then used by a Harten-Lax-van Leer-Contact Riemann solver ([Toro et al. 1994](#)). The code is capable of advecting any number of scalar quantities such as metallicity, and we add our own scalar quantity to track r-process enrichment.

The Initial Conditions for our simulations were provided by MUlti-Scale Initial Condition generator (MUSIC, [Hahn & Abel 2011](#)). The adopted Λ CDM cosmology parameters are based on Planck 2013 ([Collaboration et al. 2014](#)) $\Omega_m = 0.308$, $\Omega_b = 0.048$, $\Omega_\Lambda = 0.693$, $\sigma_8 = 0.823$ and $n = 0.96$, where the Hubble constant is $H_0 = 100h \text{ km s}^{-1} \text{ Mpc}^{-1}$ with $h = 0.678$. The simulation volume, halo mass, and stellar particle mass were all chosen as described below.

The stellar mass and circular velocity of Ret II are measured to be $\approx 5 \times 10^3 M_\odot$ and $\approx 35 \text{ km/s}$, respectively ([Roediger et al. 2016](#)). The star formation histories of UFDs indicate that nearly 3/4 of the entire stellar mass content of such galaxies is formed by $z \approx 10$ and $\approx 80\%$ of the stellar mass content is already formed by $z \approx 6$ ([Brown et al. 2014](#)). Thus we conducted an initial simulation of a volume was chosen to be 2Mpc/h, which is over 10 times the non-linear length scale at $z \approx 6$, and a resolution of 256^3 .

Within this volume, dark matter halos were found through the HOP algorithm ([Eisenstein & Hut 1998](#)). The current halo masses of UFDs are uncertain and believed to be within $10^8 - 10^9 M_\odot$ depending on the assumed dark matter density profile ([Simon & Geha 2007](#); [Bovill & Ricotti 2009](#); [Bland-Hawthorn et al. 2015](#)). [Bland-Hawthorn et al. \(2015\)](#) suggest that $M = 10^7 M_\odot$ at $z = z_{\text{reion}}$ is the minimum halo

mass that could correspond to the local UFDs such that the star formation can accumulate enough stellar mass prior to reionization and assemble a gravitational potential well deep enough to survive a SN blast. Thus we selected two halos with masses $\approx 10^8 M_\odot$ at $z = 6$ as our UFD candidate progenitors in order to capture the minimum variance in our results due to star formation histories.

After selecting the candidate halos, we performed a zoom simulation on two of the candidates. The Lagrangian box sizes within the parent 8 (Mpc/h)^3 that we re-simulated for two of the candidate halos are $246 \times 308 \times 253 \text{ (kpc/h)}^3$ and $449 \times 644 \times 609 \text{ (kpc/h)}^3$. The dark matter particles were refined to effective values 1024^3 (64 times finer in mass). The dark matter particle mass in the zoom regions is $676 M_\odot$.

The stellar mass particle is $m_* = \rho_{\text{th}} \Delta x_{\text{min}}^3 N$ where Δx_{min} is the best resolution cell size achievable and N is drawn from a Poisson distribution

$$P(N) = \frac{\bar{N}}{N!} \exp(-\bar{N}), \quad (1)$$

where

$$\bar{N} = \frac{\rho \Delta x^3}{\rho_{\text{th}} \Delta x_{\text{min}}^3} \epsilon_*, \quad (2)$$

where the star formation efficiency ϵ_* was set to 0.01 ([Krumholz & Tan 2007](#)) in our simulations. Setting $L_{\text{max}} = 19$ together with $n_* = 10 \text{ H/cm}^3$ as the threshold for the star formation in the cells results in the stellar particle mass of $\approx 50 M_\odot$, a value that allows us to resolve the stellar mass content of such systems, while still being massive enough to host the two supernovae needed to create a neutron star binary. L_{max} is the maximum refinement level that is allowed in the simulation. The adopted value was 19 which given the box of 2 Mpc/h on each side corresponds to a resolution of 5.5 pc that is kept at all redshifts.

We adopted a delayed cooling scheme for the SN feedback as discussed in [Stinson et al. \(2006\)](#) and [Dubois et al. \(2015\)](#), with a dissipation time scale of 5×10^4 years to resolve the cooling radius of the SN Sedov phase given the spatial resolution in our simulations which is $\approx 5.5 \text{ pc}$. Cooling was modeled following [Dopita & Sutherland \(1996\)](#) for $T > 10^4 \text{ K}$. Below $T = 10^4 \text{ K}$, down to 2.8 K, we adopt metal-line cooling from CLOUDY ([Ferland et al. 1998](#)).

Star formation was limited to sites with overdensities $\Delta > 200$ to avoid the formation of stars in non-virialized structures. Following the [Kroupa \(2001\)](#) Initial Mass Function (IMF), a 100 solar mass stellar particle hosts one SNcc on average. To properly model the statistics of SNe, we followed Poisson statistics with the mean number of isolated SNe equal to $N_{\text{Isolated}} = (1 - P_{\text{NSM}}) \times m_*/100 M_\odot$ and the mean number of pair SNe equal to $N_{\text{Pair}} = P_{\text{NSM}} \times m_*/200 M_\odot$. Here, P_{NSM} captures the probability that a newly formed massive star has a companion in the same mass range, such that they make a neutron star merger (NSM) in a coalescence timescale (t_{coalesce}).

A range of different values for $P_{\text{NSM}} (\approx 10^{-4} - 10^{-5})$ has been studied in [Argast et al. \(2004\)](#). However, as the stellar mass content of Reticulum II is only $\approx 5 \times 10^3 M_\odot$, we carry out our simulations such that one NSM event occurs in the star formation history of our galaxies which effectively means $P_{\text{NSM}} = 2 \times 10^{-2}$. The occurrence of only one such event is suggested by [Ji et al. \(2016\)](#) given the observed statistics of such systems in the MW halo. We carry

out simulations with three different coalescence time for t_{coalesce} (=1, 3 and 10 Myr). As our result turned out to be not sensitive to coalescence time within this range, we only present our results for t_{coalesce} (=1 and 10 Myr).

In this study, we assumed that only massive short lived stars contributed to the production of *r*-process elements and slow *s*-process channels were not modeled. Consequently we did not model elements such as Ba that have both *r*-process and *s*-process origin. Also, we did not model SN Ia because of their long delay times of the order of 200-500 Myr (Raskin et al. 2009). Given the stellar particle mass ($\approx 50M_{\odot}$), 50% of all the stellar particles were assumed to host one SNcc. The SNcc were assigned stochastically to each stellar particle. Therefore half of the stellar particles have 1 SNcc ejecting ($M_{\text{ejecta}} = 10M_{\odot}$) with a kinetic energy of $E_{\text{SN}} = 10^{51}\text{erg}$, 10 Myr after the star is formed. The metallicity yield for each SNcc is set to $\eta_{\text{SN}} = 0.1$, meaning one solar mass of metals is ejected in each SNcc event and we assume 5.4% of all the metals ejected is in the form of Fe which is consistent with the composition of IGM gas at $z \approx 6$ (private communications with Frank Timmes). There is a large uncertainty for the yields at redshifts of reionization and we instead modeled our yields in agreement with high redshifts observations of gas composition instead of the local fits. Therefore effectively every stellar particle that hosts a SNcc ejects $M_{\text{Fe}} = 0.054M_{\odot}$ into the ISM. Comparing to the iron yield from different stellar masses (Woosley & Weaver 1995) which is summarized with the following fitting formula (Shen et al. 2015)

$$M_{\text{Fe}} = 2.802 \times 10^{-4} \left(\frac{m_*}{M_{\odot}} \right)^{1.864} M_{\odot}, \quad (3)$$

our yield is similar to a yield from a 16 M_{\odot} star. It should be noted that we did not model Pop III stars or assign a different yield to them (e.g. Sarmiento et al. 2017).

Finally we explored a range of NSM models, varying the energy (E_{NSM}), coalescence timescale (t_{coalesce}), and ejected mass of *r*-process material (M_r) associated with the merger. In particular, the parameter space covered in this study is

- Three different values of the NSM energy, $E_{\text{NSM}} = 10^{50}$, 3×10^{50} , and 10^{51}erg that captures the range of kinetic energies released in a NSM event as studied in SPH simulations by Piran et al. (2013) for a range of neutron star masses ($1M_{\odot} - 2M_{\odot}$) with negligible spin parameter. This parameter impacts the spread of *r*-process elements in the host galaxy and determines the dispersion of enriched stars with *r*-process elements in the galaxy.

- Two different coalescence timescales for neutron star mergers, $t_{\text{coalesce}} = 1$ and 10 Myr. 10 Myr after a star is born, a SNcc occurs, or two SNcc in the case of the NSM particle. The coalescence time refers to the time after this explosion of the 2 SNcc. The lower limit is suggested by Belczynski et al. (2002) for their theory regarding new short-lived NS-NS sub-population, which are tight binaries with very short merger times. Moreover, binary systems with short initial separation in highly eccentric orbits can also lead to such short coalescence timescale (Korobkin et al. 2012). While much longer timescales are possible (e.g. Dominik et al. 2012), we set the maximum at 10 Myrs for this study because larger timescales ($\gtrsim 30$ Myr) would lead the NSM event to occur a system with a much larger stellar mass than Ret II given the star formation history of the halos that we simulated.

There is rather large range of *r*-process mass (M_r) possible to be ejected in a NSM event. The minimum value, $M_r = 10^{-4}M_{\odot}$, is set from results of SPH simulation of neutron star mergers by Oechslin et al. (2002) which take into account general relativistic effects in a conformally flat approximation, and the maximum value ($\approx 4 \times 10^{-2}M_{\odot}$) was set by two different SPH simulations (Korobkin et al. 2012; Piran et al. 2013)¹. With semi-newtonian potentials for NS-NS and NS-BH mergers, Just et al. (2015) studied the fate of NS mergers and found an ejecta mass of $\approx 0.004 - 0.02M_{\odot}$ and $0.035 - 0.08M_{\odot}$ for NS-BH mergers which is consistent with fully relativistic simulations of NSMs (Wanajo et al. 2014). Utilizing relativistic hydrodynamic simulations, Goriely et al. (2011) predict $M_r \approx 10^{-3} - 10^{-2}M_{\odot}$ making them the main source of elements with mass number $A > 140$ for merger rates of 10^{-5}yr^{-1} . Since M_r has no significant impact on the dynamics of the simulations, we studied this parameter in post-processing.

We stopped our simulations when the stellar content of the galaxy reaches $\approx 10^4M_{\odot}$ and assumed that further star formation will be quenched by reionization (Efstathiou 1992; Quinn et al. 1996; Klypin et al. 1999). The proper treatment of reionization would require a larger box than used in this study (e.g. box size $\approx 100\text{Mpc}$) which would be computationally prohibitive given the needed spatial resolution. Given this mismatch, it is impossible to carry out simulations of sufficiently high resolution to track single NS-NS mergers, and also self-consistently select galaxies whose overall star-formation terminates at the desired mass at the moment the wave of reionization overtakes their local environments. For this reason, simply terminating the star formation is taken as the best possible approximation to the full process.

Moreover, as we will show in (Safarzadeh & Ji, in prep), halos with mass $\log M \approx 7.5M_{\odot}$ at $z \approx 8$ have $\approx 10\%$ probability to survive as UFDs in MW progenitors. This result is based on merger tree analysis carried on the Caterpillar suite of zoom-in simulations (Griffen et al. 2016) on MW type halos and is consistent with the results presented previously in Gnedin & Kravtsov (2006). Therefore the halos selected in this study could be considered as having properties typical of the $\approx 10\%$ of faint high-redshift dwarfs that survive to be observed as present day UFDs.

3 RESULTS

Our fiducial simulation parameters are $E_{\text{NSM}} = 1 \times 10^{50}\text{erg}$, $t_{\text{coalesce}} = 10$ Myr, and $M_r = 10^{-3}M_{\odot}$. We simulate two separate halos: one in which the star formation starts at $z \approx 8$ and the other in which star formation starts at $z \approx 13$. In both cases the stellar mass of the galaxy reaches that of Ret II after ≈ 30 Myr.

We convert the total *r*-process mass ejected into the ISM by a NSM event to Europium (Eu) abundance as 97.8% of all Eu is produced by the *r*-process (see table 5 of Burris et al. 2000). Fully relativistic simulations of NS mergers by (Korobkin et al. 2012) have shown that the electron fraction (Y_e) of the ejecta can have a rather large (≈ 2) dex impact on

¹ See Table 1 of Piran et al. (2013) for the range of *r*-process material that is ejected in a NS binary simulation given the masses of each individual neutron star.

the abundance of an element like Europium. However, the abundance of r-process elements is robust to the changes in properties of the NSM event such as the binary mass ratio in a NS-NS merger with a low Y_e (≈ 0.04). The solar abundance of Eu is $A(\text{Eu}) = 0.52$ (Asplund et al. 2009) in the notation of $A(X) = \log(N(X)/N(\text{H})) + 12$ and the mass fraction of Eu in total r-process mass ejected in a NSM event is (Burris et al. 2000; Argast et al. 2004):

$$f_{\text{Eu}} = \frac{N_{\text{Eu}}^r \cdot \langle m_{\text{Eu}} \rangle}{\sum_i N_i^r \cdot \langle m_i \rangle} \approx 1.2 \times 10^{-2}, \quad (4)$$

where N_i is the number fraction of r-process nuclei of the nuclear species i , and $\langle m_i \rangle$ corresponds to mean atomic weight. The sum goes over all elements beyond Ba. In this work we have assumed all the Eu is generated in a single NSM event and the contribution from core-collapse supernovae is considered negligible. Matteucci et al. (2014) have shown that neutron star mergers alone can explain both the gradient of the [Eu/H] along the galactic center and the production of Eu in MW. They suggest the coalescence timescale to be not longer than 1 Myr and the Eu yield per NSM event to be $\approx 2 \times 10^{-7} M_{\odot}$. However, when they include the possibility of SNcc contribution to Eu production, coalescence timescales between 10-100 Myr are possible with similar Eu yield. In our simulations, given the fiducial total r-process mass that is ejected in a single NSM event to be $M_r = 10^{-3} M_{\odot}$, we are effectively assuming a Eu yield of $1.2 \times 10^{-5} M_{\odot}$ which is about 2 orders of magnitude larger than Matteucci et al. (2014) suggest. However, assuming two orders of magnitude less Eu would result in too low [Eu/H] for our stellar particles (even for the system at $z \approx 7$) to match the RetII system.

Figure 1 shows the distribution of gas-phase, metals, and r-process elements in a simulated galaxy at $z = 7.13$ with ≈ 360 stellar particles. Here the six panels illustrate the effect of varying the E_{NSM} and t_{coalesce} of the neutron star merger. Each row shows the result of increasing the E_{NSM} from 10^{50} to 10^{51} erg for a specific value of t_{coalesce} . The red contours show the [Eu/H] and the black contours show [Fe/H] of the gas. The NSM is a stellar particle with a specific ID number that is the same for all simulations, however the assignment of SNcc to stellar particles is done in a stochastic fashion and therefore the contours of [Fe/H] can be different for each simulation. The colorbar shows the projected gas density in units of gr/cm^3 . This figure should be compared to our Figure 4 which we come into shortly.

Figure 2 shows the stellar particles in [Eu/H]-[Fe/H] plane. The red points are the nine brightest stars in Ret II (Ji et al. 2016) which consist of seven detections and two upper limits. The two most metal poor stars are upper limits on [Eu/H] (indicated as downward triangles), which might be indicative of multiple star formation epochs (Webster et al. 2015). In all cases [Eu/H] and [Fe/H] are positively correlated, which is consistent with the observations (Burris et al. 2000).

The positive correlation between [Eu/H] and [Fe/H] is due the fact that the NSM event and SNcc events are spatially correlated, in that both types of events happen in the dense part of the galaxy. As stars with high [Eu/H] are those that form near the NSM, this means that they are also formed in regions that are highly-enriched with SNcc material. Note that this trend can only be captured by modeling

the spatial distribution of the ejecta. In fact, we expect no correlation between [Eu/H] and [Fe/H] if the spatial location of the NSM event is not related to the SNcc events, even if these occur at the same time. We show this point in more detail below, presenting the results of the second halo we have analyzed.

In all simulations, we have adopted a fiducial value for the injected total r-process mass in a NSM event of $10^{-3} M_{\odot}$. However, the suggested range based on GR simulations of neutron star mergers spans the range between $10^{-4} - 4 \times 10^{-2} M_{\odot}$. We therefore move the stellar particles in [Eu/H] accordingly to find the best P value that could be achieved by performing a 2D KS test against the seven detections (not including the two stars with upper limits on [Eu/H]). The stellar particles' Eu abundance is plotted for the value of M_r that results in the best P value. In all cases we get a P value of ≈ 0.1 and therefore can not reject any of our models or prefer one over the rest. However, we see that higher values of M_r in the plausible range of $10^{-4} - 4 \times 10^{-2} M_{\odot}$ are preferred to match the observations. We only consider stars with $[\text{Fe}/\text{H}] > -4$ for the KS test.

Our choice of parameters for the box size and stellar mass are chosen to resolve the Ret II dark matter halo and stellar content. At our fiducial resolution, the stellar particles have a mass of about $50 M_{\odot}$. Going one level lower in resolution would result in stellar particles larger in mass by a factor of 8, which would prevent us from resolving the stellar content of the Ret II. Therefore to do the resolution study, we carried out the same simulation but this time with $L_{\text{max}} = 18$ compared to 19. This corresponds to a resolution of ≈ 11 pc compared to 5.5 pc. Since the stellar particle mass becomes 8 times more massive ($\sim 400 M_{\odot}$), we decrease the threshold density for the star formation from $n_* = 10 \text{ H}/\text{cm}^3$ to $1.25 \text{ H}/\text{cm}^3$ to have the same mass for our stellar particles as our fiducial runs. This lower value for the threshold of star formation naturally leads to the formation of stars at earlier times. Figure 3 compares the results of our fiducial simulation (left panel) and the low resolution simulation (right panel) at $z = 7.26$. As is shown, the results of r-process enhancement are little changed. Stellar particles are enriched to the same level of enhancement with $\log(M_r/M_{\odot}) = -1.9$. Figure 3 shows the stellar particle r-process enhancement when we model the case with $E_{\text{NSM}} = 10^{51}$ erg and $t_{\text{coalesce}} = 1$ Myr with a lower resolution. The result for the lower resolution study is for the galaxy at $z = 7.26$ with 155 stellar particles formed up to that redshift.

We note that the turbulent cascades that lead to mixing in nature (Pan & Scannapieco 2010) may not be sufficiently well captured if the AMR hierarchy is truncated at too low a maximum refinement level, possibly leading to over mixing of enriched material between cells (Iapichino et al. 2008; Iapichino & Niemeyer 2008).

In order to capture the minimum variance of our results, we performed the same suite of zoom simulations on another halo, in which star formation begins at higher redshifts. Figure 4 shows the distribution of gas, metals, and r-process elements in our higher-redshift galaxy at $z = 12.3$. Note that the spatial extent of the iron and r-process elements is larger than in the galaxy presented in Figure 1. This is due to the peculiar star formation history of this galaxy, which begins as two merging clumps of gas that start forming stars within a few Myrs of each other. The NSM occurs

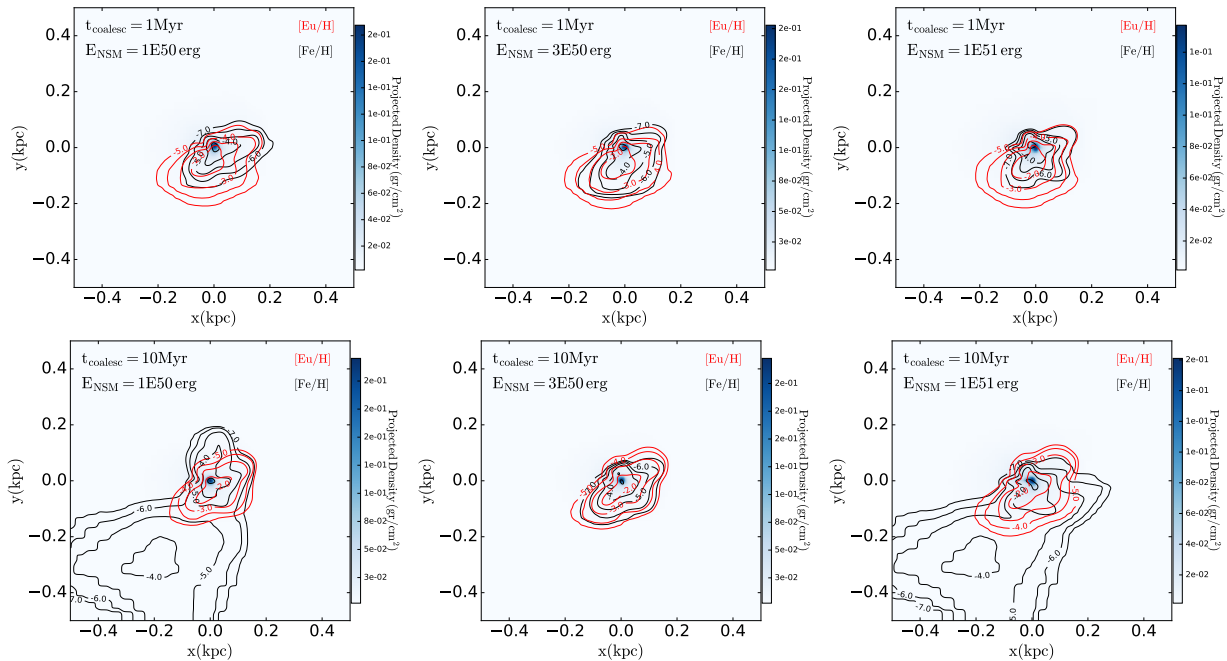


Figure 1. The projected density of our UFD candidate at $z = 7.13$. Overlaid are contours of the gas phase abundances of $[\text{Fe}/\text{H}]$ (black) and $[\text{Eu}/\text{H}]$ (red). From left to right $E_{\text{NSM}} = 10^{50}$, 3×10^{50} , and 10^{51} erg and from top to bottom $t_{\text{coalesce}} = 1$ and 10 Myr. In all cases the *r*-process material mass ejected in a NSM is set to $M_r = 10^{-3} M_{\odot}$. When $t_{\text{coalesce}} = 1$ Myr, the NSM occurs at $z = 7.4$, therefore when $t_{\text{coalesce}} = 10$ Myr, the NSM occurs 9 Myr after $z = 7.4$. The NSM is a specific particle that is tagged in our simulation and therefore unique for a given set of simulation, however the assignment of SNcc to stellar particles is done in a stochastic fashion and therefore the contours of $[\text{Fe}/\text{H}]$ can be different for each simulation.

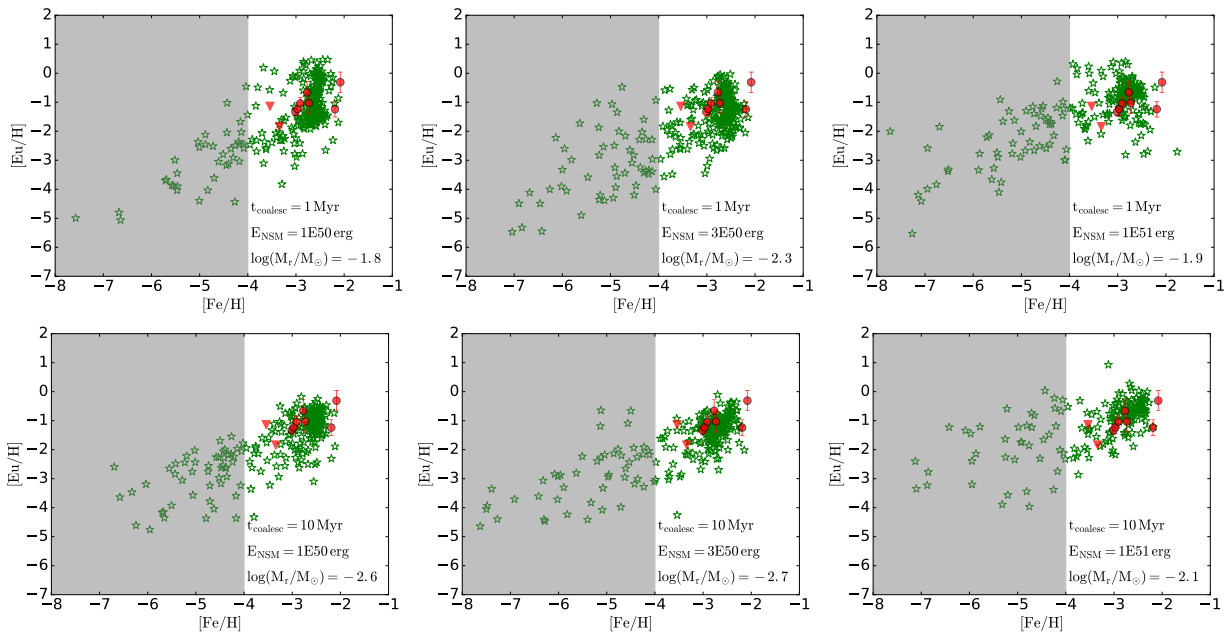


Figure 2. The $[\text{Eu}/\text{H}]$ versus $[\text{Fe}/\text{H}]$ for the stellar particles for our system at $z = 7.13$ (open green stars) vs the seven stars heavily enriched by *r*-process elements observed in Ret II (solid red points, Ji et al. 2016). The two most metal-poor stars in Ret II are upper limits for $[\text{Eu}/\text{H}]$, not detections. As in Figure 1, from left to right $E_{\text{NSM}} = 10^{50}$, 3×10^{50} , and 10^{51} erg and from top to bottom $t_{\text{coalesce}} = 1$ and 10 Myr. In all cases, the *r*-process material mass ejected (M_r) in a NSM is mentioned in the panel. The M_r values are the ones that give the best 2D KS test P value when comparing the predictions and the observations in the 2D plane. The P values are all ≈ 0.1 and therefore we can not reject or prefer a model over the rest. The shaded region indicates stars that would belong to Pop III and therefore not be detectable today. The stellar particles in this region are not used to calculate the 2D KS test.

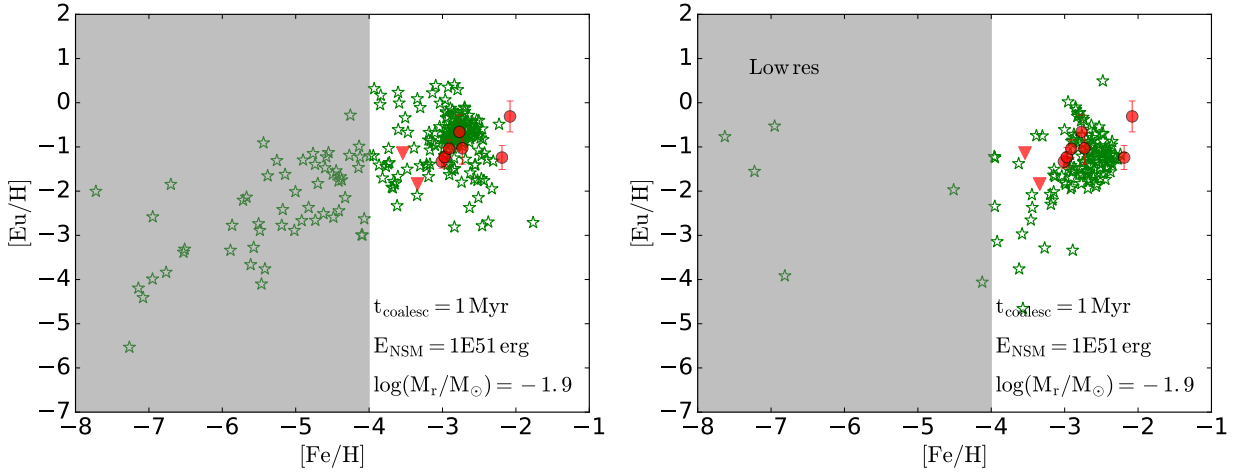


Figure 3. Showing the result of re-simulating one the case with $E_{\text{NSM}} = 10^{51}$ erg and $t_{\text{coalesce}} = 1$ Myr with our fiducial resolution on the left and with one level lower resolution corresponding to $L_{\text{max}} = 18$ on the right. Stellar particles are enriched to the same level of enhancement as for the higher resolution simulation with $\log(M_r/M_{\odot}) = -1.9$.

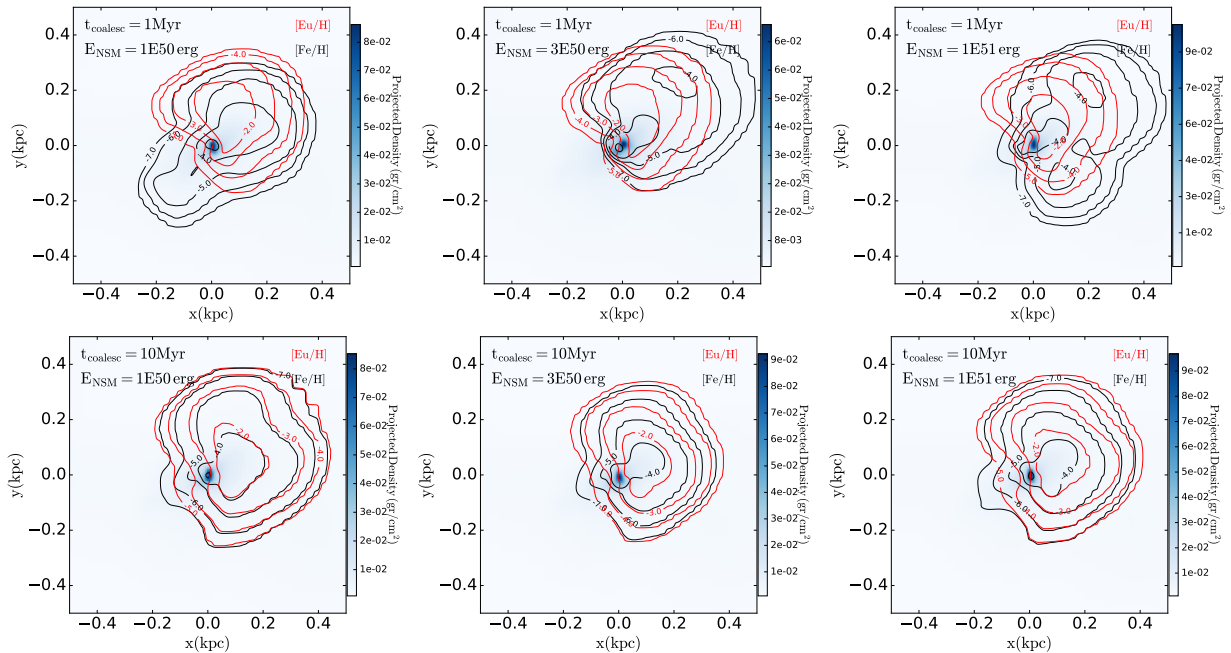


Figure 4. The projected density of our second UFD candidate at $z = 12.3$. As in Figure 1, contours of the gas phase abundances of $[\text{Fe}/\text{H}]$ (black) and $[\text{Eu}/\text{H}]$ (red) are overlaid, and from left to right and from top to bottom $E_{\text{NSM}} = 10^{50}$, 3×10^{50} , and 10^{51} erg and $t_{\text{coalesce}} = 1$ and 10 Myr respectively. Also as in Figure 1, $M_r = 10^{-3} M_{\odot}$ for all cases. In this galaxy, the off-center NSM event leads to a larger spatial distribution of ejecta, which makes the polluted gas more diluted. This leads to lower r-process enrichment of the next generation of the stars than seen in the case in which r-process material is dispersed more locally. When $t_{\text{coalesce}} = 1$ Myr, the NSM occurs at $z = 13.24$. The NSM is a specific particle that is tagged in our simulation and therefore unique for a given set of simulation, however the assignment of SNcc to stellar particles is done in a stochastic fashion and therefore the contours of $[\text{Fe}/\text{H}]$ can be different for each simulation.

in the less dense clump, and this causes the r-process elements to be dispersed over a much larger volume than if it had gone off in the dense (central) part of the potential, as was the case in the $z \approx 8$ galaxy. The unusual star formation history of this halo is illustrated in Figure 5, which shows the same halo at earlier times, when the r-process has just happened in the gas clump displaced from the densest part of the galaxy.

This leads the stellar particles to be insufficiently enriched in Eu compared to the nine stars of the Ret II as

shown in Figure 6. By performing a 2D KS test we find that we would need to inject about two orders of magnitude more r-process mass into the ISM for the NSM event to reach P values of ≈ 0.1 against the RetII data points. However, $M_r = 10^{-1} M_{\odot}$ is beyond the plausible range for the r-process mass ejecta as is suggested by the simulations. The P value with $M_r = 4 \times 10^{-2} M_{\odot}$ ranges from $\approx 10^{-3}$ to 10^{-4} for this system among different models.

Although the off-center NSM event occurs randomly in our simulation, such events could happen as a result of large

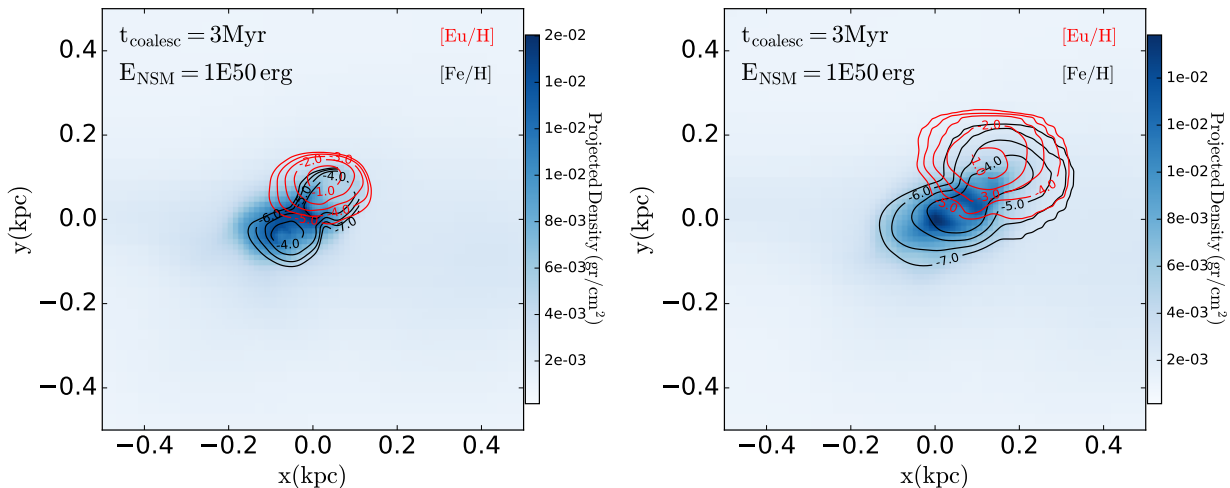


Figure 5. The same as Figure 2 but showing the results at earlier redshifts: ($z = 12.9$, left) and $z = 12.7$ (right). The NSM event happens at $z = 13.16$ in a clump of gas which is less dense than the larger clump into which it is merging. Such off-center NSM events lead to the expansion of the r-process material over a larger volume as compared with events that occur in the densest part of the galaxy. Note the expansion of the gas compared to what we observed for our lower redshift system, is more in the direction of low density region (upper-right) while the lower left extent is similar to the result for the lower redshift system.

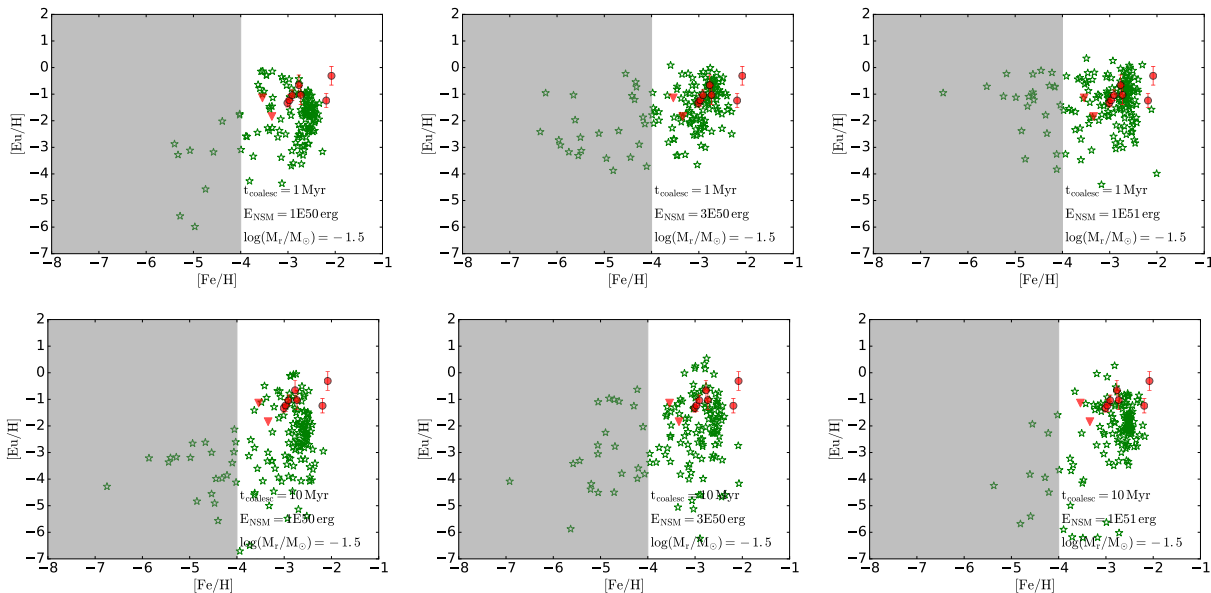


Figure 6. The same as Figure 2 but showing the results for the other system we simulated at $z = 12.3$. In all cases, the r-process material mass ejected (M_r) in a NSM is mentioned in the panel. The stellar particles are not enough enriched in Eu compared with the Ret II stars. Here we show the distribution when the best KS test result is achieved with ($\log(M_r/M_\odot) = -1.5$) which is the maximum allowed by theoretical studies. However, acceptable agreement with the data based on 2D KS test is never achieved even when we adopt the highest M_r possible. The solid red points are the nine stars in Ret II system which is a local UDF heavily enriched by r-process elements (Ji et al. 2016). Two most metal-poor stars in Ret II are upper limits for $[\text{Eu}/\text{H}]$, not detections.

natal kicks of the neutron star merger (Beniamini et al. 2016; Bramante & Linden 2016). For example in our case the spatial off-set is about 0.1 kpc, which could arise due to kicks with velocities in the range of 10 – 100 km/s assuming a typical timescale of 1-10 Myr for the system. Such high natal kicks put the NSM event well outside the dense parts of the galaxy and therefore lead to low r-process enrichment of the subsequent stars formed in the system, a picture that would not be able to explain the Ret II observations.

The impact of t_{coalesce} on the $[\text{Eu}/\text{H}]-[\text{Fe}/\text{H}]$ plane for

three different sets of star formation histories has been studied by Vangioni et al. (2016). They find that at a fixed $[\text{Fe}/\text{H}]$, higher coalescence timescales lead to lower values of $[\text{Eu}/\text{H}]$. We do not observe such trend in our simulation, in that our lower redshift system shows relatively higher values of $[\text{Eu}/\text{H}]$ at a fixed $[\text{Fe}/\text{H}]$ as the t_{coalesce} is increased. Moreover, there is no trend for our higher redshift system with t_{coalesce} but we know the off-center NSM event has had a large impact in that systems' stellar particles' abundance in $[\text{Eu}/\text{H}]-[\text{Fe}/\text{H}]$ plane. However, the coalescence timescale

studied by Vangioni et al. (2016) is 0,0.05,0.1 and 0.2 Gyr where only the $t_{\text{coalesce}}=0$ Myr case could be compared to our results. The coalescence timescale range that we have studied may not cover a wide enough range so we can observe its impact in our results. However, we can not study longer timescales because otherwise the NSM would occur after the star formation of the system has ceased and therefore we would not see any r-process enrichment in the stars.

4 SUMMARY AND CONCLUSIONS

Highly-enriched local UFDs like Ret II are perfect candidates for studying the production sites of r-process elements. Star formation in these systems is quenched by reionization such that r-process enrichment must have occurred at $z > z_{\text{reion}}$. Neutron star mergers have long been a promising candidate for the r-process element production, and for systems such as RetII, only one such event could explain the stellar abundances observed.

We performed cosmological zoom simulations of two different halos, both with a mass of $M_H \approx 10^8 M_\odot$ at $z = 6$. Each included one NSM at the very early stages of its star formation history, modeled as a stellar particle that hosts two SNcc, creating a neutron star binary that merges at a time t_{coalesce} time later. We chose a star particle mass $\approx 50 M_\odot$ to both resolve the stellar content of the RetII like system ($\approx 10^4 M_\odot$) and make it possible for a single particle to host the two SNcc events required to produce a NSM. Since the stellar particle mass in our simulation was small, we modeled supernova feedback stochastically for all the other stellar particles in the system, with a SNcc occurring 50% of the time. We modeled the NSM event with two variables: the energy of the NSM event (E_{NSM}), which we varied between $10^{50} - 10^{51}$ erg, and the coalescence timescale (t_{coalesce}) that we varied between 1 and 10 Myr. When post-processing our simulations, we allowed the amount of r-process material released into the ISM in a NSM event to vary between $10^{-4} M_\odot$ and $4 \times 10^{-2} M_\odot$, with a fiducial values of $10^{-3} M_\odot$, and we converted the r-process content to europium, the primary element that is almost solely produced in r-process events. The Eu yield adopted in this study is comparable to what Vangioni et al. (2016) had implemented ($7 \times 10^{-5} M_\odot$) by considering the yields from both the binary merger phase and the BH-torus evolutions.

Our results show that a single NSM can lead to a distribution of stellar r-process abundances similar to those observed in Ret II. In one of the two halos that we simulated, the NSM event took place at the center of the stellar distribution, leading to a high spatial correlation between the r-process material and the supernovae ejecta. This not only lead to high-levels of r-process enrichment such as seen in Ret II, but also the positive correlation between [Eu/H] and [Fe/H]. In the second halo, the NSM event took place away from the densest part of the galaxy, and the r-process material expanded primarily into the low density ISM. In this case, the more extended and shallower r-process distribution lead to stars that were on average about 2 dex under-abundant in europium as compared with Ret II stars. Although even in this case we still see some of the stars with high levels enrichment comparable to those of Ret II, our simulations show that even without modeling the natal

kicks, the binary can explode in places that would lead to very inefficient r-process enrichment in the system.

Thus it is the location of NSM event, rather than the ejection energy or the coalescence delay time scale, that is the dominant parameter in determining the r-process distribution in ultra faint dwarf galaxies. This means that hydrodynamic simulations, such as the one carried out in this study are required to reliably interpret measurements of r-process enhanced metal poor stars. It also means that the natal kicks of neutron stars, which were not modeled in this study, are likely to play in important role in determining these abundances. Further theoretical modeling of this processes is needed to better understand the r-process enrichment of local ultra-faint dwarf galaxies.

Recently, Hansen et al. (2017) reported a discovery of a star with [Eu/H]=-1.65 and [Fe/H]=-2.25 in Tucana III. The stellar particles in our simulation cover a wide range in [Eu/H] -[Fe/H] plane and the star that Hansen et al. (2017) observed lies where we have simulated stars to match its abundance. Both our high and low redshift simulated UFD's stars easily overlap with this star, therefore we can not exclude the possibility that a NSM merger is also responsible for its enrichment. However more than one star is required to have a sufficient statistics to robustly constrain the origin of r-process enhancement in Tucana III.

Objects with $v_{\text{peak}} \leq 25 \text{ km s}^{-1}$ and $M_{\text{peak}} > 10^{7.5} M_\odot$ are potential candidates to survive as present day UFDs. All "peak" quantities are defined as occurring at the time at which a halo's main branch reaches its maximum mass; i.e. M_{peak} is the maximum mass of a halo, and v_{peak} is v_{max} at that time. This criterion is set to define these systems as true fossils in that they never reached a mass scale in their entire history large enough to be able to accrete gas from IGM and therefore reignite star formation and be considered as polluted systems (Gnedin & Kravtsov 2006; Bovill & Ricotti 2011). To see whether our simulated dwarfs will survive as present day UFDs, it would be necessary to follow their evolution down to $z = 0$. Moreover the candidates would need to be selected from a MW progenitor. In a parallel paper (Safarzadeh & Ji, in prep) we will present the statistics of such systems on the probability of a random selection of a $10^8 M_\odot$ halo at $z=6$ to survive as a present day UFD. The probabilities are about $\sim 10\%$ consistent with Gnedin & Kravtsov (2006).

Short gamma ray bursts (sGRBs) are believed to be the result of neutron star mergers and the coalescence timescales considered in this study are on the short end of the allowed range based on sGRB observations (Berger 2010) and population synthesis models. The coalescence time can be very long, (e.g. Dominik et al. 2012) and the delay time distributions could be modeled as a power law ($\propto t^{-1}$) with minimum timescale of 1 Myr and maximum of 10 Gyr. Clearly if the NSM occurs after the star formation history of the system has ceased due to re-ionization, then there would be no sign of r-process enrichment in the stars of such a UFD. It can be that NSM has occurred in other UFDs but at a time at which there is no subsequent star formation. We have shown that the dominant variable is the location of the NSM in the system, which determines the subsequent enrichment of the newly born stars. Moreover, not only the coalescence timescale, but also the natal kick distribution would

impact the possibility of r-process enrichment in a system. This combined effect will be explored in future work.

5 ACKNOWLEDGEMENTS

We are thankful to the anonymous referee for their careful reading of our manuscript. We are thankful to Frank Timmes, Alexander Ji, Mark Richardson and Rick Sarmiento for useful discussions. We used the yt package (Turk et al. 2011) and pynbody (Pontzen et al. 2013) for part of the analysis in this work. This work was supported by the National Science Foundation under grant AST14-07835 and by NASA under theory grant NNX15AK82G. We would also like to thank the Texas Advanced Computing Center (TACC) at The University of Texas at Austin, and the Extreme Science and Engineering Discovery Environment (XSEDE) for providing HPC resources via grant TG-AST130021 and TG-AST160063 that have contributed to the results reported within this paper.

REFERENCES

- Argast D., Samland M., Thielemann F. K., Qian Y. Z., 2004, *Astronomy & Astrophysics*, 416, 997
- Asplund M., Grevesse N., Sauval A. J., Scott P., 2009, *Annual Review of Astronomy and Astrophysics*, 47, 481
- Bechtol K., et al., 2015, *The Astrophysical Journal*, 807, 50
- Belczynski K., Kalogera V., Bulik T., 2002, *The Astrophysical Journal*, 572, 407
- Beniamini P., Hotokezaka K., Piran T., 2016, *The Astrophysical Journal Letters*, 829, L13
- Berger E., 2010, *The Astrophysical Journal*, 722, 1946
- Bland-Hawthorn J., Sutherland R., Webster D., 2015, *The Astrophysical Journal*, 807, 154
- Bovill M. S., Ricotti M., 2009, *The Astrophysical Journal*, 693, 1859
- Bovill M. S., Ricotti M., 2011, *The Astrophysical Journal*, 741, 17
- Bramante J., Linden T., 2016, *The Astrophysical Journal*, 826, 57
- Brown T. M., et al., 2012, *The Astrophysical Journal Letters*, 753, L21
- Brown T. M., et al., 2014, *The Astrophysical Journal*, 796, 91
- Burbidge E. M., Burbidge G. R., Fowler W. A., Hoyle F., 1957, *Reviews of Modern Physics*, 29, 547
- Burris D. L., Pilachowski C. A., Armandroff T. E., Sneden C., Cowan J. J., Roe H., 2000, *The Astrophysical Journal*, 544, 302
- Busso M., Gallino R., Wasserburg G. J., 1999, *Annual Review of Astronomy and Astrophysics*, 37, 239
- Collaboration P., et al., 2014, *Astronomy & Astrophysics*, 571, A16
- Cowan J. J., Thielemann F.-K., Truran J. W., 1991, *Physics Reports*, 208, 267
- Dominik M., Belczynski K., Fryer C., Holz D. E., Berti E., Bulik T., Mandel I., O’Shaughnessy R., 2012, *The Astrophysical Journal*, 759, 52
- Dopita M. A., Sutherland R. S., 1996, *ApJS*, 102, 161
- Dubois Y., Volonteri M., Silk J., Devriendt J., Slyz A., Teyssier R., 2015, *Monthly Notices of the Royal Astronomical Society*, 452, 1502
- Efstathiou G., 1992, *Monthly Notices of the Royal Astronomical Society*, 256, 43P
- Eisenstein D. J., Hut P., 1998, *The Astrophysical Journal*, 498, 137
- Ferland G. J., Korista K. T., Verner D. A., Ferguson J. W., Kingdon J. B., Verner E. M., 1998, *Publications of the Astronomical Society of the Pacific*, 110, 761
- Frebel A., Bromm V., 2012, *The Astrophysical Journal*, 759, 115
- Gnedin N. Y., Kravtsov A. V., 2006, *The Astrophysical Journal*, 645, 1054
- Goriely S., Bauswein A., Janka H.-T., 2011, *The Astrophysical Journal Letters*, 738, L32
- Griffen B. F., Ji A. P., Dooley G. A., Gómez F. A., Vogelsberger M., O’Shea B. W., Frebel A., 2016, *ApJ*, 818, 10
- Hahn O., Abel T., 2011, *Monthly Notices of the Royal Astronomical Society*, 415, 2101
- Hansen T. T., et al., 2017, *The Astrophysical Journal*, 838, 44
- Iapichino L., Niemeyer J. C., 2008, *Monthly Notices of the Royal Astronomical Society*, 388, 1089
- Iapichino L., Adamek J., Schmidt W., Niemeyer J. C., 2008, *Monthly Notices of the Royal Astronomical Society*, 388, 1079
- Ji A. P., Frebel A., Chiti A., Simon J. D., 2016, *Nature*, 531, 610
- Just O., Bauswein A., Pulpillo R. A., Goriely S., Janka H. T., 2015, *Monthly Notices of the Royal Astronomical Society*, 448, 541
- Klypin A., Kravtsov A. V., Valenzuela O., Prada F., 1999, *The Astrophysical Journal*, 522, 82
- Koposov S. E., Belokurov V., Torrealba G., Evans N. W., 2015a, *The Astrophysical Journal*, 805, 130
- Koposov S. E., et al., 2015b, *The Astrophysical Journal*, 811, 62
- Korobkin O., Rosswog S., Arcones A., Winteler C., 2012, *Monthly Notices of the Royal Astronomical Society*, 426, 1940
- Kroupa P., 2001, *Monthly Notices of the Royal Astronomical Society*, 322, 231
- Krumholz M. R., Tan J. C., 2007, *The Astrophysical Journal*, 654, 304
- Kuroda T., Wanajo S., Nomoto K., 2008, *The Astrophysical Journal*, 672, 1068
- Matteucci F., Romano D., Arcones A., Korobkin O., Rosswog S., 2014, *Monthly Notices of the Royal Astronomical Society*, 438, 2177
- Nishimura N., Takiwaki T., Thielemann F.-K., 2015, *The Astrophysical Journal*, 810, 109
- Oechslin R., Rosswog S., Thielemann F.-K., 2002, *Physical Review D*, 65, 103005
- Pan L., Scannapieco E., 2010, *The Astrophysical Journal*, 721, 1765
- Piran T., Nakar E., Rosswog S., 2013, *Monthly Notices of the Royal Astronomical Society*, 430, 2121
- Pontzen A., Roskar R., Stinson G., Woods R., 2013, *Astrophysics Source Code Library*, p. ascl:1305.002
- Quinn T., Katz N., Efstathiou G., 1996, *Monthly Notices of the Royal Astronomical Society*, 278, L49
- Raskin C., Scannapieco E., Rhoads J., Della Valle M., 2009, *The Astrophysical Journal*, 707, 74
- Roederer I. U., et al., 2016, *The Astronomical Journal*, 151, 82
- Rosswog S., Liebendörfer M., Thielemann F. K., Davies M. B., Benz W., Piran T., 1999, *Astronomy & Astrophysics*, 341, 499
- Rosswog S., Davies M. B., Thielemann F. K., Piran T., 2000, *MNRAS*, 360, 171
- Sarmiento R., Scannapieco E., Pan L., 2017, *The Astrophysical Journal*, 834, 23
- Shen S., Cooke R. J., Ramirez-Ruiz E., Madau P., Mayer L., Guedes J., 2015, *The Astrophysical Journal*, 807, 115
- Simon J. D., Geha M., 2007, *The Astrophysical Journal*, 670, 313
- Sneden C., Cowan J. J., 2003, *Science*, 299, 70
- Sneden C., Cowan J. J., Gallino R., 2008, *Annual Review of Astronomy and Astrophysics*, 46, 241
- Stinson G., Seth A., Katz N., Wadsley J., Governato F., Quinn T., 2006, *Monthly Notices of the Royal Astronomical Society*,

- 373, 1074
- Tanvir N. R., Levan A. J., Fruchter A. S., Hjorth J., Hounsell R. A., Wiersema K., Tunnicliffe R. L., 2013, *Nature*, 500, 547
- Teyssier R., 2002, *Astronomy & Astrophysics*, 385, 337
- Toro E. F., Spruce M., Speares W., 1994, *Shock Waves*, 4, 25
- Turk M. J., Smith B. D., Oishi J. S., Skory S., Skillman S. W., Abel T., Norman M. L., 2011, *The Astrophysical Journal Supplement*, 192, 9
- Vangioni E., Goriely S., Daigne F., François P., Belczynski K., 2016, *Monthly Notices of the Royal Astronomical Society*, 455, 17
- Vargas L. C., Geha M., Kirby E. N., Simon J. D., 2013, *The Astrophysical Journal*, 767, 134
- Wallner A., et al., 2015, *Nature Communications*, 6, 5956
- Wanajo S., 2013, *The Astrophysical Journal*, 770, L22
- Wanajo S., Sekiguchi Y., Nishimura N., Kiuchi K., Kyutoku K., Shibata M., 2014, *The Astrophysical Journal Letters*, 789, L39
- Webster D., Bland-Hawthorn J., Sutherland R., 2015, *The Astrophysical Journal Letters*, 799, L21
- Wehmeyer B., Pignatari M., Thielemann F. K., 2015, *Monthly Notices of the Royal Astronomical Society*, 452, 1970
- Winteler C., Käppeli R., Perego A., Arcones A., Vasset N., Nishimura N., Liebendörfer M., Thielemann F. K., 2012, *The Astrophysical Journal Letters*, 750, L22
- Woosley S. E., Weaver T. A., 1995, *ApJS*, 101, 181
- Woosley S. E., Wilson J. R., Mathews G. J., Hoffman R. D., Meyer B. S., 1994, *Astrophysical Journal*, 433, 229
- van de Voort F., Quataert E., Hopkins P. F., Kereš D., Faucher-Giguère C.-A., 2015, *Monthly Notices of the Royal Astronomical Society*, 447, 140

This paper has been typeset from a $\text{\TeX}/\text{\LaTeX}$ file prepared by the author.